Quantum Electronics **49** (2) 169–177 (2019) ©2019 Kvantovaya Elektronika and Turpion Ltd

https://doi.org/10.1070/QEL16720

Theoretical simulation of a signal for a scheme of an atomic spin gyroscope with optical detection

E.N. Popov, K.A. Barantsev, A.N. Litvinov

Abstract. **An operation scheme of an atomic spin gyroscope with optical detection is described, in which two noble gas isotopes, ^{129}Xe and ^{131}Xe, are used as carriers of the spin of an atomic nucleus. Based on this scheme, we construct a theoretical model of the dynamics of the spin polarisation of an alkali metal and the magnetisation of a noble gas under conditions of spin-exchange interaction and optical pumping. This model allows one to simulate the pumping and signal readout in the gyroscope scheme. The time dependences of this signal are plotted, the analysis of which shows that the signal has a sophisticated complex structure. Thus, the problem arises of demodulating this signal based on the improvement of demodulation methods and algorithms.**

Keywords: *laser gyroscope, atomic spin, optical detection.*

1. Introduction

Recently, much attention has been paid to the development of high-precision navigation systems. Presently, in the world today there are two global navigation systems that provide communication anywhere on the planet: GLONASS and GPS. These systems have certain disadvantages, the main of which is the requirement that there be no obstacles in the path of signal transmission between the satellite and the navigation receiver (client). This significantly limits the applicability of these systems in places where it is difficult to receive a signal from satellite navigation systems. In such cases, the so-called inertial navigation systems are used, which determine the location of the object using the fundamental properties of the inertia of motion in noninertial reference systems during turns and linear acceleration. The advantages of inertial navigation systems are autonomy, versatility and noise immunity. In aviation, space, sea and geodesic systems (where there is no signal from GLONASS and GPS systems), the current location, speed and direction of movement of an object can be only determined by using inertial navigation systems. To stabilise the course of motion in such systems use is made of gyroscopes.

E.N. Popov, K.A. Barantsev, A.N. Litvinov Peter the Great St. Petersburg Polytechnic University, ul. Politecknicheskaya 29, 195251 St. Petersburg, Russia;
e-mail: enp-tion@yandex.ru, andrey.litvinov@mail.ru

Received 8 May 2018; revision received 3 July 2018
Kvantovaya Elektronika **49** (2) 169–177 (2019)
Translated by I.A. Ulitkin

The effect of nuclear magnetic resonance (NMR) is resonant absorption or radiation at a certain frequency (NMR frequency) of electromagnetic energy by a substance containing nuclei with nonzero spin in an external magnetic field, which is caused by the reorientation of the magnetic moments of the nuclei [1]. The use of this effect gave rise to whole directions in physics (spin echo [2], quantum magnetometers [3]), chemistry (chemical shift, spin–spin interaction [4]) and medicine (magnetic resonance imaging [5]) associated with nuclear spectroscopy. Nuclear spin can play the role of a quantum mechanical top that is not subjected to friction or other mechanical effects. One of the most popular methods for measuring the angular velocity is the generation of a torque, which causes the nuclear spin to perform precession around a selected axis with a certain angular velocity in the laboratory reference frame. Then, in the rotating reference frame of a quantum gyroscope, another value of angular velocity will be detected, different from the angular velocity in the laboratory system, which is preserved. The difference in detected angular velocities in these reference systems makes it possible to determine the speed with which the sensor itself rotates. According to this principle, a NMR-based gyroscope operates [6–9].

The first working NMR-based scheme for measuring the angular velocity of rotation was implemented in mercury vapour containing ^{199}Hg and ^{201}Hg isotopes with different gyromagnetic ratios [10, 11]. The idea was that the Larmor precession frequencies for two isotopes in the same external magnetic field are different. In this scheme, the precession frequencies (corresponding to each of the isotopes) in the gyroscope reference system can be measured directly in the device using a modulator and a frequency metre. With the algebraic exception of induction of an external magnetic field, it is possible to obtain a mechanical frequency of rotation. The use of two isotopes makes the scheme resistant to fluctuations of the magnetic field and gives an advantage over similar schemes working with a single carrier of atomic spin. However, due to the complexity of miniaturisation and numerous technological problems associated with mercury use, this scheme is not effective for practical use.

Kornack at al. [12] suggested a scheme of a quantum rotation sensor based on an atomic co-magnetometer, which has several advantages over the above-mentioned NMR scheme for a mixture of two gases with different gyromagnetic ratios of the nuclei. This scheme is fundamentally different from the mercury gyro scheme, since it artificially suppresses the spin-exchange interaction between an alkali metal and a noble gas

and does not use magnetic resonance. In the co-magnetometer scheme, the electron spin of alkali metal atoms is pumped by circularly polarised laser radiation and transmitted to the noble gas atoms through the spin-exchange interaction during collisions [13]. However, the technical complexity of the implementation of the co-magnetometer and the insufficient development of the theory in this direction makes it less popular than the NMR-based quantum gyroscope. Moreover, a significant drawback of such a device is the very high sensitivity of the gyroscope to changes in the angle between the pump and readout beams; there is also a problem associated with the need for a high degree of protection from external magnetic fields and for a precise setting of the compensating magnetic field.

There is another alternative scheme of a quantum rotation sensor on a nuclear spin, which is not implemented in practice. This scheme, described in [14], is physically close to the NMR sensor scheme on two xenon isotopes, but it uses one circularly polarised laser beam both for pumping and for reading. At the same time, the alternative scheme has a significant drawback, i.e. complexity of laser parameter optimisation, due to the fact that different intensities, polarisations and detunings are required for pumping and reading.

A more advanced NMR-based scheme for measuring the angular velocity was implemented in 2011 by an American company, Northrop Grumman [15–18]. At the same time, we should note that the work of Northrop Grumman was a continuation of the Litton Industries work, which began in the 1970s. Later Litton Industries later became part of Northrop Grumman. In contrast to the mercury spin generator, in this scheme two noble gas isotopes – ^{129}Xe and ^{131}Xe – were used. The main advantage of xenon is a large cross section of the spin-exchange interaction, the presence of two stable isotopes (^{129}Xe and ^{131}Xe) with a spin not exceeding 3/2, and g-factors of different signs. In addition, both isotopes with nonzero angular momenta are contained in sufficient quantities in natural xenon gas. As a result, in 2014, the following characteristics of the device were achieved: a drift of 0.02 deg h^{-1}, and an angle random walk (ARW) of 0.005 deg h$^{-1/2}$ [18, 19]. In terms of the drift, the fabricated device does not fully correspond to the navigation class. The next task is to improve the processing (demodulation) of the signal and to reduce the influence of temperature and magnetic gradients on the accuracy of its measurement. Optimisation of these values is one of the key problems. Simultaneously with the research conducted in the USA on the making of a NMR-based gyroscope, scientists from China have been engaged in this direction in recent years. At present, they also use the scheme of pumping nuclear spins through the spin-exchange interaction with alkali metal atoms. As the noble gases in this scheme use is made of two stable xenon isotopes [20, 21].

The main advantage of this scheme is the possibility of its miniaturisation in using vertical-cavity surface emitting lasers (VCSELs) for pumping and reading. In addition, working with a noble gas instead of mercury seems to be simpler in terms of the technical implementation of the device. An essential argument in favour of choosing such a scheme is the fact that the prototype of the device, albeit with insufficient characteristics for the navigation class, has already been implemented. Thus, the objective of this paper is to develop a theoretical model of the dynamics of nuclear magnetisation of two noble-gas isotopes in the scheme of an atomic spin gyroscope with optical detection [in the literature on this subject it is customary to call it an NMR-based gyroscope (NMR-gyro)], which would make it possible to take into account all main physical effects that appear during the implementation of this gyroscope. As a result, the theoretical model should provide an opportunity to simulate the signal of a physical gyroscope unit and to carry out multifactor optimisation of the gyroscope parameters in order to achieve the navigation accuracy class.

2. Description and principle of NMR-gyro operation

Consider the basic principle of NMR-gyro operation. The main physical unit of the gyroscope is a cell containing two isotopes of a noble gas, a saturated alkali metal vapour and a nitrogen buffer gas. Two noble-gas isotopes, ^{129}Xe and ^{131}Xe, in which the gyromagnetic ratios of the nuclei are different, are used as carriers of the nuclear spin.

Since all the electron shells of xenon atoms are filled and do not interact with light, an alkali metal (Rb or Cs) is used to pump and read out the polarisation of xenon. The spin polarisation between alkali atoms and xenon isotopes is transferred through the spin-exchange interaction. To increase the efficiency of this interaction, the nitrogen buffer gas (N_2) is additionally used, which also allows the fluorescence of alkali atoms to be quenched.

Optical pumping of alkali atoms in the working medium produces a dedicated direction of polarisation, which is transmitted from the alkali metal to xenon through collisions and spin-exchange interaction. The transverse radio frequency field applied to the cell allows the NMR of both xenon isotopes to be excited. Since the gyromagnetic ratios of the ^{129}Xe and ^{131}Xe isotopes differ in sign, the Larmor precession occurs for them in opposite directions. Then, the measured precession frequencies of xenon isotopes in a gyroscope's reference frame rotating at speed Ω can be expressed as

$$\begin{aligned} \omega_{129} &= \gamma_{129} B_0 - \Omega, \\ \omega_{131} &= \gamma_{131} B_0 + \Omega. \end{aligned} \tag{1}$$

From (1) it is clear that by eliminating algebraically the external magnetic field B_0 we can determine the value of Ω. In this case, the comparison of the sum frequency

$$\omega_0 = \omega_{129} + \omega_{131} = (\gamma_{129} + \gamma_{131}) B_0 \tag{2}$$

with the reference frequency makes it possible to stabilise a constant external magnetic field B_0 by the feedback to the coil. The use of external magnetic shielding allows NMR-gyro to be poorly susceptible to the magnetic field fluctuations.

Let us now examine in more detail the scheme of the sensitive NMR-gyro element (Fig. 1). Thus, we will make use of a cell (*3*) containing a gas mixture of two isotopes, an alkali metal and a buffer gas. Note that the concentration of alkali atoms is approximately six orders of magnitude lower than the concentration of xenon and nitrogen. We will apply to the cell a constant volume-uniform longitudinal magnetic field (*4*), which will determine the precession frequencies of nuclear magnetisation of both isotopes (^{129}Xe and ^{131}Xe) and

the resonant frequency of the electron paramagnetic resonance of the alkali metal atoms. Then the vector (*2*) of nuclear magnetisation of the noble gas will perform a precession motion (*1*) around the magnetic induction vector. Now we apply two transverse magnetic fields (*5*) to the cell at the NMR frequency of two xenon isotopes – ^{129}Xe and ^{131}Xe. It is also necessary to apply an alternating magnetic field along the axis of the pump beam, produced by the coil (*6*) and causing the longitudinal electron paramagnetic resonance (EPR) of an alkali metal. VCSEL-type compact laser sources are used as a pumping and detecting laser [22]. For optical pumping, we use circularly polarised laser radiation (*7*), tuned to resonance with one of the transitions of the alkali metal D_1 line. The propagation direction of the laser pump coincides with the direction of the magnetic induction vector generated by the coil (*6*). The detecting beam (*8*) is located perpendicular to the pump beam and has a linear polarisation. As the detecting beam passes through the cell, the angle ψ of inclination of the polarisation plane to the z axis changes due to the inverse paramagnetic Faraday effect. Before entering the cell, the polarisation plane (*9*) is perpendicular to the xy plane. Finally, the radiation of the detecting beam is incident on the polarisation divider (*10*), which splits the detecting beam into two beams whose polarisation planes are rotated by angles of +45° and –45° around the propagation axis of the detecting beam relative to its original polarisation plane.

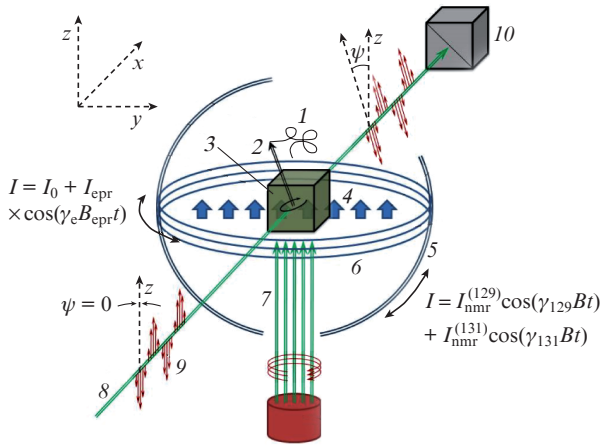

Figure 1. Schematic of the sensitive MNR-gyro element: I_0 is the direct current flowing in the coils and producing a longitudinal magnetic field B_0 along the z axis; I_{epr} is the alternating current flowing in coils and producing a longitudinal alternating magnetic field B_{epr}; $I_{nmr}^{(129)}$ and $I_{nmr}^{(131)}$ are the alternating currents flowing in the coils and producing a transverse alternating magnetic field B, which causes NMR in ^{129}Xe and ^{131}Xe, respectively; ψ is the angle of inclination of the polarisation plane to the z axis (for the other notation see the text).

Thus, by changing the angle of inclination of the polarisation plane of the detecting beam as it passes through the cell, we can determine the angular velocity of the mechanical rotation Ω. It should be noted that since the beam of the detecting laser is split into two orthogonally polarised beams and the difference between their intensities is measured, the noise arising on a photodetector should be compared with the signal, which can be several orders of magnitude less, rather than with the intensity of the detecting radiation. This leads to an additional requirement for the characteristics of the detection scheme: It must have as little noise as possible to achieve the navigation accuracy class of the NMR-gyro.

It should be noted that the implementation of the gyro scheme is further complicated by two circumstances. First, it is the need to provide a whole complex (more than ten) of sensitive feedbacks [23]. Secondly, since the signal measured at the photodetector (the angle of inclination of the polarisation plane to the z axis) is of a sophisticated nature, it is needed to develop new methods for demodulating the existing signal [24].

Let us turn to the mathematical description of the scheme presented in Fig. 1 and try to construct the NMR-gyro theory, which takes into account all the basic physical processes occurring during pumping and reading of the spin polarisation in a gas cell containing a mixture of alkaline atoms, xenon isotopes and a nitrogen buffer gas.

3. Mathematical model of the atomic spin gyroscope

In order to mathematically describe the scheme shown in Fig. 1, we consider separately the equations for pumping alkali atoms and the dynamics of isotopes of a noble gas. A connecting link between these equations will be the constant of the spin-exchange interaction. We first turn our attention to alkaline atoms interacting with the pump, $\boldsymbol{E}^{\mathrm{p}}(z,t)$, and readout, $\boldsymbol{E}^{\mathrm{s}}(z,t)$, fields. In this case, the electric field is represented in the form of a classical plane wave and the scheme of alkali metal levels is considered to be quantum-mechanical. This is the so-called semi-classical approach, which has proven itself in describing such systems [25, 26]. Further, we use the frequency ω as the reference frequency, corresponding to the difference in the arithmetic mean energies of the excited hyperfine sublevels in the D_1 line and the upper hyperfine alkaline metal sublevel in the ground state of the electron shell $2S_{1/2}$.

The intensity of the electric field of the pump propagating along the x axis can be expressed as:

$$\boldsymbol{E}^{\mathrm{p}}(z,t) = E_0^{\mathrm{p}}\boldsymbol{e}_{\mathrm{p}}\exp[-\mathrm{i}(\omega t + \delta_{\mathrm{p}} t - k_{\mathrm{p}} z)] + \text{c.c.}, \quad (3)$$

where E_0^{p} is the amplitude of the pump field; $\boldsymbol{e}_{\mathrm{p}}$ is the unit polarisation vector (in a circular basis it can be decomposed into vectors $\boldsymbol{e}_{\pm}$, corresponding to left- and right-hand circular polarisations); δ_{p} is the single photon detuning of the pump field; and k_{p} is the wave number.

Similarly, we write the expression for the field of scanning radiation propagating along the z axis:

$$\boldsymbol{E}^{\mathrm{s}}(x,t) = E_0^{\mathrm{s}}\boldsymbol{e}_{\mathrm{s}}\exp[-\mathrm{i}(\omega t + \delta_{\mathrm{s}} t - k_{\mathrm{s}} x)] + \text{c.c.}, \quad (4)$$

where E_0^{s} is the amplitude of the readout field; $\boldsymbol{e}_{\mathrm{s}}$ is the unit polarisation vector; δ_{s} is the single photon detuning of the readout field; and k_{s} is the wave number.

We will describe the state of an alkaline atom by the density matrix $\rho_{\alpha\beta}(\boldsymbol{v},\boldsymbol{r},t)$, where $\boldsymbol{v}$ and $\boldsymbol{r}$ are the velocity and coordinate of the atom in the laboratory reference frame. Quantum kinetic equations for the density matrix have the form

$$\left(\frac{\partial}{\partial t} + \boldsymbol{v}\nabla\right)\rho_{\alpha\beta}(\boldsymbol{v},\boldsymbol{r},t)$$

$$= -\frac{\mathrm{i}}{\hbar}\sum_{j=1}^{N}[H_{\alpha j}\rho_{j\beta}(\boldsymbol{v},\boldsymbol{r},t) - \rho_{\alpha j}(\boldsymbol{v},\boldsymbol{r},t)H_{j\beta}] + R_{\alpha\beta} + S_{\alpha\beta}, \quad (5)$$

where $\hat{H}$ is the Hamiltonian of the interaction of an alkaline atom with a laser field; R is the relaxation matrix; and S is the collision integral. The Hamiltonian can be represented as $\hat{H} = \hat{H}_0 + \hat{V}$, where

$$\hat{H}_0 = \sum_i \varepsilon_i |i\rangle \langle i| \tag{6}$$

is the Hamiltonian in the absence of a laser field (ε_i is the energy of the alkaline atom levels); and the operator $\hat{V}$ describes the interaction of an atom with a laser field. In the dipole approximation,

$$\hat{V} = \hat{V}^{\mathrm{p}} + \hat{V}^{\mathrm{s}} + \gamma_{\mathrm{e}} \sum_{n,F} g_{nF} \hat{S}_{nF} \boldsymbol{B}(t), \tag{7}$$

where $\hat{V}^{\mathrm{p}} = -\hat{d}\boldsymbol{E}^{\mathrm{p}}$; $\hat{V}^{\mathrm{s}} = -\hat{d}\boldsymbol{E}^{\mathrm{s}}$; $\hat{d}$ is the operator of the alkali metal dipole moment; γ_{e} is the gyromagnetic ratio of an alkali atom; g_{nF} is the Landé factor for the corresponding energy level n and the total angular momentum F; $\hat{S}_{nF}$ are the Pauli spin matrices for the total angular momentum corresponding to the energy level of the alkali atom n; and $\boldsymbol{B}(t)$ is the magnetic field vector, which is a superposition of magnetic fields applied to the cell. Next we will consider it in more detail.

We turn to the basis of hyperfine states. We divide the density matrix $\hat{\sigma}$ in this basis into submatrices, which will describe the two lower hyperfine levels ($\hat{\sigma}_{\mathrm{gg}}$) and the two upper hyperfine sublevels ($\hat{\sigma}_{\mathrm{ee}}$) in the D_1 lines and the optical coherence between them ($\hat{\sigma}_{\mathrm{eg}}$) under the assumption that the radio frequency and Zeeman coherences $\hat{\sigma}_{\mathrm{gg}'}$ and $\hat{\sigma}_{\mathrm{ee}'}$ are zero. We assume that the atomic density matrix due to the Doppler effect depends on the projections of their velocities on the axes of the laser beams and on the coordinates along them; therefore, $\sigma \equiv \sigma(x, z, v_x, v_z, t)$, and the pumping is organised from the level with $F_{\mathrm{g}} = 2$ to levels with $F_{\mathrm{e}} = 1, 2$.

We select the slowly varying components of the optical coherence produced by the pump and readout fields, which we denote as $\sigma^{\mathrm{p}}_{\mathrm{eg}}(\boldsymbol{v}, \boldsymbol{r}, t)$ and $\sigma^{\mathrm{s}}_{\mathrm{eg}}(\boldsymbol{v}, \boldsymbol{r}, t)$, respectively:

$$\rho_{\mathrm{eg}}(\boldsymbol{v}, \boldsymbol{r}, t) = \exp(\mathrm{i}\omega t + \mathrm{i}\delta_{\mathrm{p}} t - \mathrm{i}k_{\mathrm{p}} z)\sigma^{\mathrm{p}}_{\mathrm{eg}}(\boldsymbol{v}, \boldsymbol{r}, t) + \exp(\mathrm{i}\omega t + \mathrm{i}\delta_{\mathrm{s}} t - \mathrm{i}k_{\mathrm{s}} x)\sigma^{\mathrm{s}}_{\mathrm{eg}}(\boldsymbol{v}, \boldsymbol{r}, t). \tag{8}$$

The work considers the distribution of alkali metal atoms in velocities, which, at thermodynamic equilibrium, exactly coincides with the Maxwell distribution:

$$\mu_v(v_x, v_z) = \left[\frac{1}{v_0\sqrt{\pi}} \exp\left(-\frac{v_z^2}{v_0^2}\right)\right]\left[\frac{1}{v_0\sqrt{\pi}} \exp\left(-\frac{v_x^2}{v_0^2}\right)\right], \tag{9}$$

where $v_0 = \sqrt{2k_{\mathrm{B}}T/m_{\mathrm{a}}}$; k_{B} is the Boltzmann constant; T is the cell temperature; and m_{a} is the mass of an alkali metal atom. Due to the fact that atoms have relatively high velocities (since $T = 55\,^{\circ}\mathrm{C} - 80\,^{\circ}\mathrm{C}$), we neglect the collective polyatomic effects observed for cold atomic ensembles [27–29].

Next, we perform integration over velocities under the assumption that maxwellisation occurs during collisions. Then the dynamic system of equations for the matrix $\hat{\sigma}$, describing an alkaline atom in the ground and excited states, which interacts with the pump and readout fields, will have the form:

$$\frac{\partial \hat{\sigma}_{\mathrm{gg}}}{\partial t} - D_{\mathrm{gg}}\left(\frac{\partial^2 \hat{\sigma}_{\mathrm{gg}}}{\partial x^2} + \frac{\partial^2 \hat{\sigma}_{\mathrm{gg}}}{\partial y^2} + \frac{\partial^2 \hat{\sigma}_{\mathrm{gg}}}{\partial z^2}\right) = \mathrm{i}(\hat{V}^{\mathrm{p}}_{\mathrm{gg}} \times \hat{\sigma}_{\mathrm{gg}} - \hat{\sigma}_{\mathrm{gg}} \times \hat{V}^{\mathrm{p}}_{\mathrm{gg}} + \hat{V}^{\mathrm{s}}_{\mathrm{ge}} \times \hat{\sigma}^{\mathrm{s}}_{\mathrm{eg}} - \hat{\sigma}^{\mathrm{s}}_{\mathrm{ge}} \times \hat{V}^{\mathrm{s}}_{\mathrm{eg}} + \hat{V}^{\mathrm{p}}_{\mathrm{ge}} \times \hat{\sigma}_{\mathrm{eg}} - \hat{\sigma}_{\mathrm{ge}} \times \hat{V}^{\mathrm{p}}_{\mathrm{eg}}) + \mathrm{i}\mu\left\{\left[\sum_{\alpha = x,y,z} B_\alpha(t)\hat{S}_\alpha\right] \times \hat{\sigma}_{\mathrm{gg}} - \hat{\sigma}_{\mathrm{gg}} \times \left[\sum_{\alpha = x,y,z} B_\alpha(t)\hat{S}_\alpha\right]\right\} + \mathrm{i}\mu_{\mathrm{shift}} B_0(\hat{S}_{\mathrm{shift}} \times \hat{\sigma}_{\mathrm{gg}} - \hat{\sigma}_{\mathrm{gg}} \times \hat{S}_{\mathrm{shift}}) + \frac{1}{2}\mathcal{R}(\hat{P}_1 \times \Im\{\hat{\sigma}_{\mathrm{ee}}, \hat{I}_G\} \times \hat{P}_1 + \hat{P}_2 \times \Im\{\hat{\sigma}_{\mathrm{ee}}, \hat{I}_G\} \times \hat{P}_2) - \mathcal{F}\left(\hat{\sigma}_{\mathrm{gg}} - \frac{1}{G}\hat{I}_G\right), \tag{10}$$

$$\frac{\partial \hat{\sigma}_{\mathrm{ee}}}{\partial t} - D_{\mathrm{ee}}\left(\frac{\partial^2 \hat{\sigma}_{\mathrm{ee}}}{\partial x^2} + \frac{\partial^2 \hat{\sigma}_{\mathrm{ee}}}{\partial y^2} + \frac{\partial^2 \hat{\sigma}_{\mathrm{ee}}}{\partial z^2}\right) = \mathrm{i}(\hat{V}^{\mathrm{p}}_{\mathrm{ee}} \times \hat{\sigma}_{\mathrm{ee}} - \hat{\sigma}_{\mathrm{ee}} \times \hat{V}^{\mathrm{p}}_{\mathrm{ee}} + \hat{V}^{\mathrm{s}}_{\mathrm{eg}} \times \hat{\sigma}_{\mathrm{ge}} - \hat{\sigma}^{\mathrm{s}}_{\mathrm{eg}} \times \hat{V}^{\mathrm{s}}_{\mathrm{ge}} + \hat{V}^{\mathrm{p}}_{\mathrm{eg}} \times \hat{\sigma}_{\mathrm{ge}} - \hat{\sigma}_{\mathrm{eg}} \times \hat{V}^{\mathrm{p}}_{\mathrm{ge}}) + \mathrm{i}\frac{\mu}{3}\left\{\left[\sum_{\alpha = x,y,z} B_\alpha(t)\hat{S}_\alpha\right] \times \hat{\sigma}_{\mathrm{ee}} - \hat{\sigma}_{\mathrm{ee}} \times \left[\sum_{\alpha = x,y,z} B_\alpha(t)\hat{S}_\alpha\right]\right\} - (\mathcal{R} + \mathcal{F})\hat{\sigma}_{\mathrm{ee}} - \nu_{\mathrm{mix}}\left(\hat{\sigma}_{\mathrm{ee}} - \frac{1}{2}\Im\{\hat{\sigma}_{\mathrm{ee}}, \hat{I}_G\}\right), \tag{11}$$

$$\nu_{\mathrm{dec}}\hat{\sigma}^{\mathrm{p}}_{\mathrm{ge}} - \mathrm{i}\int_{-\infty}^{+\infty}[\hat{V}^{\mathrm{p}}_{\mathrm{gg}} \times \hat{\sigma}^{\mathrm{p}}_{\mathrm{ge}}(v_x, v_z) - \hat{\sigma}^{\mathrm{p}}_{\mathrm{ge}}(v_x, v_z) \times \hat{V}^{\mathrm{p}}_{\mathrm{ee}}]\mathrm{d}v_x\mathrm{d}v_z = \mathrm{i}\int_{-\infty}^{+\infty}\mu_v(v_x, v_z)(\hat{V}^{\mathrm{p}}_{\mathrm{ge}} \times \hat{\sigma}_{\mathrm{ee}} - \hat{\sigma}_{\mathrm{gg}} \times \hat{V}^{\mathrm{p}}_{\mathrm{ge}})\mathrm{d}v_x\mathrm{d}v_z, \tag{12}$$

$$\nu_{\mathrm{dec}}\hat{\sigma}^{\mathrm{s}}_{\mathrm{ge}} - \mathrm{i}\int_{-\infty}^{+\infty}[\hat{V}^{\mathrm{s}}_{\mathrm{gg}} \times \hat{\sigma}^{\mathrm{s}}_{\mathrm{ge}}(v_x, v_z) - \hat{\sigma}^{\mathrm{s}}_{\mathrm{ge}}(v_x, v_z) \times \hat{V}^{\mathrm{s}}_{\mathrm{ee}}]\mathrm{d}v_x\mathrm{d}v_z = \mathrm{i}\int_{-\infty}^{+\infty}\mu_v(v_x, v_z)(\hat{V}^{\mathrm{s}}_{\mathrm{ge}} \times \hat{\sigma}_{\mathrm{ee}} - \hat{\sigma}_{\mathrm{gg}} \times \hat{V}^{s}_{\mathrm{ge}})\mathrm{d}v_x\mathrm{d}v_z. \tag{13}$$

Here, $D_{\alpha\alpha}$ is the diffusion coefficient in the cell at specified partial pressures in the mixture; ν_{dec} is the relaxation rate of optical coherence; ν_{mix} is the rate of mixing between Zeeman levels in the excited state; $\hat{V}^{\mathrm{p}}_{\mathrm{gg}}$ is a submatrix of the alkali metal interaction operator with the pump field, containing detuning of the pump field:

$$\hat{V}^{\mathrm{p}}_{\mathrm{gg}} = \begin{pmatrix} 0 \times \hat{I}_{G_1} & 0 \\ 0 & \delta_{\mathrm{p}} \times \hat{I}_{G_2} \end{pmatrix} + kv_z\hat{I}_G; \tag{14}$$

$\hat{V}^{\mathrm{s}}_{\mathrm{gg}}$ is a submatrix of an alkali metal interaction operator with a readout field, containing detuning of the readout field:

$$\hat{V}^{\mathrm{s}}_{\mathrm{gg}} = \begin{pmatrix} (\delta_{\mathrm{s}} + \omega_{\mathrm{hfsg}})\hat{I}_{G_1} & 0 \\ 0 & \delta_{\mathrm{s}}\hat{I}_{G_2} \end{pmatrix} + kv_x\hat{I}_G; \tag{15}$$

ω_{hfsg} is the hyperfine splitting in the ground state; $\hat{V}^{\mathrm{p}}_{\mathrm{ee}}$ is a submatrix that allows one to take into account the hyperfine splitting ω_{hfse} of the excited level in the D_1 line:

$$\hat{V}^{\mathrm{p}}_{\mathrm{ee}} = \begin{pmatrix} \frac{\omega_{\mathrm{hfse}}}{2}\hat{I}_{G_1} & 0 \\ 0 & -\frac{\omega_{\mathrm{hfse}}}{2}\hat{I}_{G_2} \end{pmatrix}; \tag{16}$$

$\hat{V}^{\mathrm{p}}_{\mathrm{ge}}$ is a submatrix of the alkali metal interaction operator with the pump field, which contains the amplitude and polarisation of the field (the ± sign defines the left- or right-handed circular polarisation of the electric field):

$$\hat{V}^{\mathrm{p}}_{\mathrm{ge}} = \frac{d_{\mathrm{m}}}{\hbar}(\hat{g}^{\mathrm{p}}_{\pm}E^{\mathrm{p}}_{\pm}); \tag{17}$$

$\hat{V}^{\mathrm{s}}_{\mathrm{eg}}$ is a submatrix of an alkaline metal interaction operator with the readout field, containing the amplitude and polarisation of the field:

$$\hat{V}^{\mathrm{s}}_{\mathrm{eg}} = \frac{d_{\mathrm{m}}}{\hbar}(\hat{g}^{\mathrm{s}}_{-}E^{\mathrm{s}}_{-} + \hat{g}^{\mathrm{s}}_{+}E^{\mathrm{s}}_{+}); \tag{18}$$

$\hat{g}^{\mathrm{p}}_{\pm}$ and $\hat{g}^{\mathrm{s}}_{\pm}$ are the circular components of the dipole moment operator of the pump and readout fields, respectively:

$$\hat{g}^{\mathrm{p,s}}_{\pm} = G_{F_{\mathrm{g}}F_{\mathrm{e}}}\sum_{F_{\mathrm{g}},F_{\mathrm{e}},m,\,m'}(-1)^{F_{\mathrm{g}}-m}\begin{pmatrix} F_g & 1 & F_{\mathrm{e}} \\ -m & \pm 1 & m' \end{pmatrix}|F_{\mathrm{g}},m\rangle\langle F_{\mathrm{e}},m'|; \tag{19}$$

$$G_{F_{\mathrm{g}}F_{\mathrm{e}}} = (-1)^{F_{\mathrm{e}}+J_{\mathrm{g}}+I+1}\times\sqrt{(2F_{\mathrm{g}}+1)(2F_{\mathrm{e}}+1)}\begin{Bmatrix} I_{\mathrm{n}} & F_{\mathrm{g}} & J_{\mathrm{g}} \\ 1 & J_{\mathrm{e}} & F_{\mathrm{e}} \end{Bmatrix}, \tag{20}$$

where F_{g} and F_{e} are the total moments of the hyperfine ground ($|\mathrm{g}\rangle$) and excited ($|\mathrm{e}\rangle$) levels; m and m' are the projections of the total moment of the atom in the states $|\mathrm{g}\rangle$ and $|\mathrm{e}\rangle$, respectively; J_{g} and J_{e} are the angular moments of the electron shell; I_{n} is the angular momentum of the nucleus; d_{m} is the reduced dipole moment of the transition of the D_1 line of an alkali metal; μ is a constant defining the splitting of Zeeman levels in a magnetic field in the first order; μ_{shift} is a constant defining the splitting of Zeeman levels in a magnetic field in the second order (determined from the Breit–Rabi formula [30]); $B_\alpha(t)$ is the projection of the alternating magnetic field on the coordinate axes; $\hat{S}_\alpha$ is the Pauli matrix for the corresponding values of the angular momentum of the energy level; $\hat{S}_{\mathrm{shift}}$ is the matrix that takes into account the hyperfine splitting of the EPR frequency for different levels:

$$\hat{S}_{\mathrm{shift}} = \sum_{F,m} m\,|F,m\rangle\langle F,m|; \tag{21}$$

$G = G_1 + G_2$ is the total number of levels equal to the sum of the numbers of hyperfine sublevels G_1 and G_2; $\hat{I}_G$ is the unit matrix of rank G; and $\hat{P}_{1,2}$ are the operators of projections on the corresponding ultrafine level in the D_1 line of the alkali metal:

$$\hat{P}_1 = \begin{pmatrix} \hat{I}_{G_1} & 0 \\ 0 & 0 \end{pmatrix}_G, \tag{22}$$

$$\hat{P}_2 = \begin{pmatrix} 0 & 0 \\ 0 & \hat{I}_{G_2} \end{pmatrix}_G. \tag{23}$$

In formulae (19), (20), the circular polarisation components of the pump and readout fields are determined for different directions of the wave vector.

The constants $\mathcal{R}$ and $\mathcal{F}$ determine relaxation and are calculated using the theory of spin-exchange interaction: $\mathcal{R}$ describes the rate of transition of atoms from the excited state to the unexcited state under the action of inelastic collisions with nitrogen molecules, and $\mathcal{F}$ is the process of the spin-exchange interaction with xenon atoms [31, 32].

The relaxation of the spin polarisation of an alkali metal in an excited state, which occurs in collisions with buffer gas atoms, deserves special attention. The electron shell of a polarised atom in the excited state in the D_1 line is anisotropic; therefore, in collisions, the spatial shape of the electron shell is redistributed. This process continues until the electron shell becomes isotropic. The rate of the described depolarisation process can be estimated as the frequency of collisions with the atoms of the buffer gas. A characteristic feature of the relaxation of spin polarisation is that the time of collisions of atoms of an alkali metal and a buffer gas at the considered temperatures is only 10^{-12} s, whereas the characteristic time of interaction between the nucleus and the electron shell of an alkali metal is about 10^{-9} s. This factor leads to the fact that the relaxation of the angular momentum of the atom occurs nonuniformly: only the spin polarisation of the electron shell of the alkali metal atoms is destroyed, and the state of the nucleus remains almost unchanged. The analytical form of the superoperator $\Im\{\hat{\sigma}_{\mathrm{ee}}, \hat{I}_G\}$ of inhomogeneous relaxation to model this process in the hyperfine basis is discussed in detail in [33].

Note that optical coherences are described by a quasi-stationary approximation, in which it is assumed that the rate of destruction of optical coherences in collisions considerably exceeds the rate of other processes. Therefore, we put $\partial\hat{\sigma}_{\mathrm{eg}}/\partial t = 0$ in the equations.

In solving the system of equations (10)–(13), it is necessary to take into account that the density matrix is normalised to unity; therefore, the condition

$$\mathrm{Tr}(\hat{\sigma}_{\mathrm{gg}}) + \mathrm{Tr}(\hat{\sigma}_{\mathrm{ee}}) = 1 \tag{24}$$

is always met.

Since the NMR-gyro scheme uses fairly high concentrations of alkali atoms, the pump and readout fields are absorbed. In order to take this into account, it is necessary to supplement the system of equations (10)–(13) with Maxwell's equations for the field:

$$\frac{\partial E^{\mathrm{p}}_{\pm}(x,y,z)}{\partial z} = \mathrm{i}\frac{k_{\mathrm{p}}d_{\mathrm{m}}n_{\mathrm{c}}}{\varepsilon_0}\mathrm{Tr}[\hat{g}^{\mathrm{p}}_{\pm}\times\sigma^{\mathrm{p}}_{\mathrm{eg}}(x,y,z)], \tag{25}$$

$$\frac{\partial E^{\mathrm{s}}_{\pm}(x,y,z)}{\partial x} = \mathrm{i}\frac{k_{\mathrm{s}}d_{\mathrm{m}}n_{\mathrm{c}}}{\varepsilon_0}\mathrm{Tr}[\hat{g}^{\mathrm{s}}_{\pm}\times\sigma^{\mathrm{s}}_{\mathrm{eg}}(x,y,z)], \tag{26}$$

where n_{c} is the temperature-dependent concentration of alkali metal atoms.

To solve the system of equations (10)–(13) and (25), (26), it is necessary to set boundary conditions. We will assume that when an alkali atom collides with a wall, it undergoes a transition from the excited state to the ground state, that is, the population of the excited level is zero, and the optical coherences are destroyed. Populations of lower sublevels are aligned. Mathematically, this can be formulated as follows:

$$\hat{\sigma}_{\mathrm{gg}}|_{\mathrm{cell\ boundary}} = \frac{1}{G}\hat{I}_G, \tag{27}$$

$$\hat{\sigma}_{\mathrm{ee}}|_{\mathrm{cell\ boundary}} = \hat{\sigma}_{\mathrm{eg}}|_{\mathrm{cell\ boundary}} = 0\cdot\hat{I}_G. \tag{28}$$

For electric fields, the boundary conditions are

$$E^{\mathrm{p}}_{\pm}(x,y,z=0,t) = f^{\mathrm{p}}_{\pm}(x,y,z), \tag{29}$$

$$E^{\mathrm{s}}_{\pm}(x=0,y,z,t) = f^{\mathrm{s}}_{\pm}(y,z,t). \tag{30}$$

Let us now consider the dynamics of the nuclear polarisation of xenon isotopes, ^{129}Xe and ^{131}Xe. To describe the evolution of the spin of the noble gas nucleus, we use the mathematical apparatus based on the Bloch equations [34]. To do this, we introduce the macroscopic magnetic moment of a unit volume (magnetisation) $\boldsymbol{M}_{\xi}(t)$ produced by the ξ-isotope (ξ = 129, 131) of the gas mixture, and the symbol $M_{\xi\max}$ denotes the maximum possible magnetisation of the ξ-isotope of xenon, in which all the magnetic moments of a noble nucleus gas are parallel:

$$M_{\xi\max} = \gamma_{\xi} n_{\xi} I_{\xi} \hbar, \tag{31}$$

where γ_{ξ}, n_{ξ} and I_{ξ} are the gyromagnetic ratio of the nucleus, the concentration and the angular momentum of the ξ-isotope nucleus in the gas mixture.

The Bloch equations, taking into account relaxation processes and spin-exchange interaction, will have the form [35, 36]:

$$\frac{\mathrm{d}\boldsymbol{M}_{\xi}(t)}{\mathrm{d}t} = \gamma_{\xi}[\boldsymbol{M}_{\xi}(t)\times\boldsymbol{B}'(t)] - \Gamma_{\xi}\boldsymbol{M}_{\xi}(t)$$

$$+ \Gamma^{\mathrm{SE}}_{\xi}[M_{\xi\max}\boldsymbol{P}_{\mathrm{e}} - \boldsymbol{M}_{\xi}(t)]. \tag{32}$$

Here $\Gamma^{\mathrm{SE}}_{\xi}$ is the rate of magnetisation of the ξ-isotope of xenon during spin-exchange interaction with polarised alkali metal atoms; Γ_{ξ} is the phenomenological relaxation rate of the nuclear magnetisation of the ξ-isotope of xenon, caused by collisions with walls and binary collisions with other atoms in the cell; $\boldsymbol{B}'(t)$ is the magnetic field vector in the gas cell; and $\boldsymbol{P}_{\mathrm{e}}(t)$ is the vector of alkali metal spin polarisation averaged over the EPR period. The constants $\Gamma^{\mathrm{SE}}_{\xi}$ in equation (32) and $\mathcal{F}$ in (10)–(13) characterise the same process and are related by an algebraic expression. Due to the cumbersome nature of this expression and the complexity of the theory of spin-exchange interaction, we do not present it in this paper, but refer the reader to the original source [31, 32].

Let us consider in more detail the components of the magnetic field vector $\boldsymbol{B}(t)$. It is known that alkali metal atoms in a cell are under the action of an effective magnetic field produced by polarised xenon. In this case, the effective magnetic field is enhanced (increased by three orders of magnitude) due to the Fermi contact interaction in an alkaline atom–noble gas atom pair (the gain is usually denoted by the letter λ). This effect leads to a difference in the magnetic field inductions $\boldsymbol{B}(t)$ and $\boldsymbol{B}'(t)$ in equations (10)–(13) for an alkali metal and in equation (32) for each noble gas isotope.

As mentioned above, the gas cell is placed in a longitudinal magnetic field B_0, directed along the z axis. Also, an alternating high-frequency magnetic field with amplitude B_{epr} and frequency ω_{epr}, causing a longitudinal EPR is applied along the z axis:

$$B_z(t) = B_0 + B_{\mathrm{epr}}\sin(\omega_{\mathrm{epr}} t). \tag{33}$$

In the xy plane, a field is applied that causes the NMR of both xenon isotopes:

$$B_x(t) = \sum_{\xi} B_{x\xi}\sin(\omega_{\mathrm{nmr}\xi} t + \varphi_{x\xi}), \tag{34}$$

$$B_y(t) = \sum_{\xi} B_{y\xi}\sin(\omega_{\mathrm{nmr}\xi} t + \varphi_{y\xi}). \tag{35}$$

Here, $\omega_{\mathrm{nmr}\xi}$ is the frequency of the alternating magnetic field causing the NMR of the ξ-isotope of xenon; $B_{x\xi}$, $B_{y\xi}$ and $\varphi_{x\xi}$, $\varphi_{y\xi}$ are the amplitudes and phases, which determine the magnitude and polarization of the alternating magnetic field in the xy plane. We will assume that the magnitude and direction of the magnetic field are uniform over the entire volume of the gas mixture. This approximation may be valid for gas cells in which the time of flight of xenon atoms through the cell is much less than the lifetime of the spin of the nucleus. Due to this condition, the nuclear magnetisation of the noble gas is averaged over the volume.

Fields (33)–(35) are generated by external sources (coils) and enter into the equations for an alkali metal (10)–(13) and nuclear magnetisation (32) in the same way. We define their sum as an external magnetic field:

$$\boldsymbol{B}_{\mathrm{ext}}(t) = B_x(t)\boldsymbol{e}_x + B_y(t)\boldsymbol{e}_y + B_z(t)\boldsymbol{e}_z. \tag{36}$$

Next, we consider the fields produced in the gas cell by spin polarisations of an alkali metal and a noble gas. The spin polarisation of an alkali metal generates an additional field $\boldsymbol{B}_{\mathrm{alk}}$ that affects the precession motion of the magnetisation vector of both xenon isotopes [34]:

$$\boldsymbol{B}_{\mathrm{alk}}(t) = \mu_0 n_{\mathrm{c}} \mu_{\mathrm{B}} \lambda \boldsymbol{P}_{\mathrm{e}}(t). \tag{37}$$

Here μ_0 is the magnetic constant; and μ_{B} is the Bohr magneton. Note that the field $\boldsymbol{B}_{\mathrm{alk}}$ is directed along the spin polarisation vector of an alkali metal, the direction of which, in turn, is determined by the axis of propagation of the pump radiation. In our case, this is the z axis.

The nuclear magnetisation $\boldsymbol{M}_{\xi}(t)$ of the ξ-isotope of produces an effective magnetic field $\boldsymbol{B}_{\mathrm{eff}\xi}(t)$, which acts on an alkali metal:

$$\boldsymbol{B}_{\mathrm{eff}\xi}(t) = \mu_0 \lambda \boldsymbol{M}_{\xi}(t). \tag{38}$$

It carries information about the precession of the nuclear spin of noble gas atoms and, therefore, about the frequency of the mechanical rotation of the sensor. Now we can determine the induction of the magnetic field, which contains alkaline atoms [$\boldsymbol{B}(t)$] and xenon atoms [$\boldsymbol{B}'(t)$]:

$$\boldsymbol{B}(t) = \boldsymbol{B}_{\mathrm{ext}}(t) + \sum_{\xi} \boldsymbol{B}_{\mathrm{eff}\xi}(t), \tag{39}$$

$$\boldsymbol{B}'(t) = \boldsymbol{B}_{\mathrm{ext}}(t) + \boldsymbol{B}_{\mathrm{alk}}(t). \tag{40}$$

Thus, we can conclude that the system of equations for the alkali metal (10)–(13), (25), (26) and the Bloch equations (32), modified to take into account relaxation processes and spin-exchange interaction, essentially describe the main physical processes occurring during the NMR-gyro operation. It is worth noting that the system of equations (10)–(13), (25), (26) and (32) is self-consistent, and the relation between these equations and the transformation into a single inseparable mathematical model occurs due to both the spin-exchange interaction constant $\Gamma^{\mathrm{SE}}_{\xi}$ and mag-

netic fields $\boldsymbol{B}(t)$ and $\boldsymbol{B}'(t)$. The next step is the joint solution of this system of equations.

4. Main results

In this section, we will consider as an example the results of calculating the signal in the gyroscope scheme, obtained by jointly solving the system of equations (10)–(13), (25), (26) and (32). The rubidium atom ^{87}Rb was chosen as the alkali metal. The complexity of the calculation can be judged by different time scales of the dynamic model. The greatest time scale corresponds to the precession motion of nuclear magnetisation, the period of which is hundredths of a second. The smallest time scale corresponds to the establishment of the optical coherence of the alkali metal under the action of laser pumping, the period of which is tens of nanoseconds. We can mention a number of processes proceeding within the cell with intermediate periods: For example, the precession motion of the spin polarisation of an alkali metal, the period of which is a few microseconds. The solution of the dynamic system of equations describing a series of processes with very different rates leads to the need to consider large time intervals with a small partitioning step. This negatively affects the speed of the programme that implements the mathematical model.

Below we present the results of calculations performed under the following conditions: the ^{87}Rb atom is used as the alkali metal; the cell temperature is 70 °C (343 K); the cell has a linear size of $5 \times 5 \times 5$ cm; the pressures of the N_2 buffer gas and of each of the two isotopes (^{129}Xe and ^{131}Xe) are the same and amount to 10 Torr; magnetic field is $B_0 = 12$ μT; the field is $B_{\text{epr}} = 1.9B_0$; the right-handed circularly polarised pump radiation with intensity $I_p = 1$ mW cm^{-2} is set in the middle between the transitions $|F_g = 2\rangle \rightarrow |F_e = 1\rangle$ and $|F_g = 2\rangle \rightarrow |F_e = 2\rangle$; the linearly polarised scanning field with intensity $I_s = 1$ mW cm^{-2} is set from the middle between the levels $|F_e = 1\rangle$ and $|F_e = 2\rangle$ at $\delta_s = -4\omega_{\text{hfse}}$; the electric field profile is assumed to be constant in the transverse plane; and the magnetisation gains is $\lambda = 500$.

As mentioned above, by a gyroscope signal is meant the time dependence of the angle of inclination of the polarisation plane of the detecting beam as it passes through the cell. Figure 2 shows the NMR-gyro signal. It can be seen that it has a complex composite structure. An important conclusion from the analysis of Fig. 2 is that simple demodulation methods do not allow the values of mechanical rotation frequencies to be determined with the necessary accuracy. Thus, the serious problem of demodulating this signal is added to the purely computational problem, which was mentioned above [24]. The signal region at the EPR frequencies is poorly investigated. The complex structure of the signal suggests the possibility of improving the gyroscope characteristics, if use is made of the high-quality demodulation method with advanced algorithms. It is worth noting that standard demodulation methods do not allow one to obtain the required accuracy of the gyroscope. New demodulation algorithms will provide an opportunity to carry out multivariate optimisation and determine the parameters of the gyroscope, ensuring its navigation accuracy class.

To extract the slow precession of nuclear magnetisation containing information about the mechanical rotation of the gyroscope, it is necessary to average the signal over the EPR period, as a result of which an effective signal is obtained,

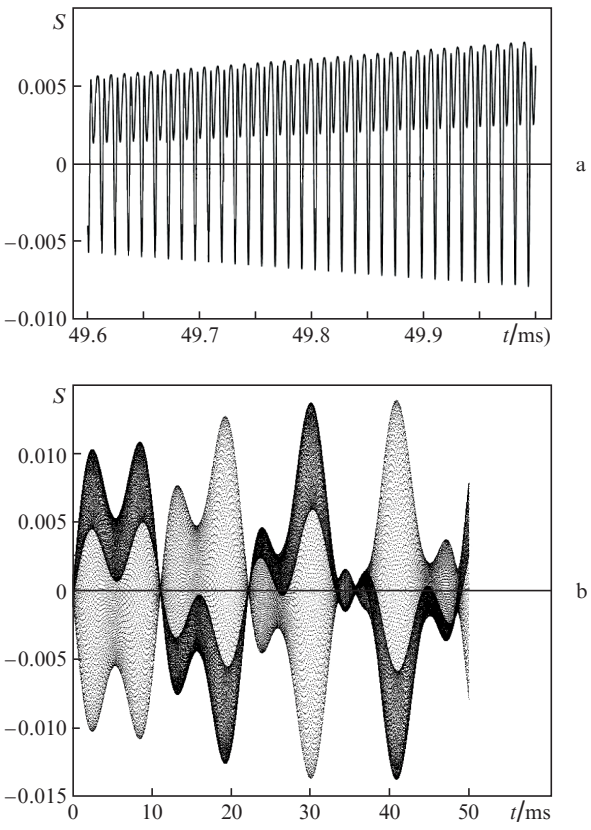

Figure 2. Gyroscope signal $S(t)$ obtained on different time scales: (a) 0.5 and (b) 50 ms.

which is shown in Fig. 3. Despite the simplicity of implementation, this approach has drawbacks associated with the appearance of phase modulation of the low-frequency xenon precession signal. Their allowance turns into a separate complex task of demodulation.

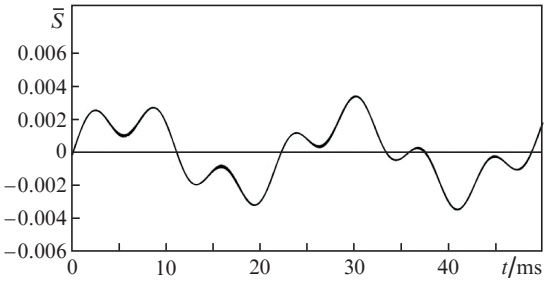

Figure 3. Signal $\overline{S(t)}$ after averaging over the EPR period, containing low-frequency components resulting from the nuclear magnetisation precession of xenon.

There is an alternative approach to signal processing that allows one to extract the precession frequencies of the nuclear magnetisation of both xenon isotopes without the higher harmonics associated with phase modulation. Its essence lies in the use of a synchronous detector at the EPR frequency, which in the signal (see Fig. 2) is the carrier frequency of fast oscillations. A synchronous detector can extract both the first and second harmonics of the EPR frequency. However, since the signal of the second harmonic is

smaller in amplitude than the signal of the first harmonic, we give as an example the simulation results of the synchronous detection of the signal of the first harmonic. Figure 4 shows the envelope of the signal, which is obtained at the output of the synchronous detector. Subsequent demodulation of this signal to extract the xenon precession frequencies is simpler than in the first case and this demodulation is used in practice.

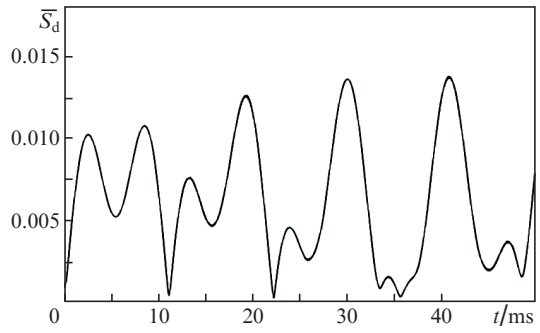

Figure 4. Amplitude of the signal $\overline{S_d(t)}$ after passing through a synchronous detector at the EPR frequency.

Thus, we can assert that the theoretical NMR-gyro model constructed in the paper allows one to simulate its signal. The number of input and output parameters of the gyroscope is about two dozen; therefore, the use of a theoretical model together with advanced signal demodulation methods make it possible to carry out multifactor optimisation, with which one can make significant progress in finding the most optimal parameters to achieve the required gyroscope accuracy.

It should be noted that the paper considers the optical pumping of an alkali metal by a single-frequency field. At the same time, the application of two optical fields can lead to the appearance of additional opportunities for optical pumping and, thereby, will increase the NMR-gyro accuracy. However, this task is much more challenging, since so-called dark states can arise in such a scheme, which, in the presence of a dense medium, can result in rotation of the polarisation plane and ellipticity of linearly polarised radiation along the x axis at the input [37]. It is likely that the use of partially correlated two-frequency radiation may provide additional opportunities for the implementation of the NMR-gyro [38].

5. Conclusions

The paper describes the scheme of an NMR-based gyroscope. Within the framework of the semi-classical approach, a theoretical model of pumping and reading the spin polarisation of an alkali metal saturated vapour in a cell has been developed. Using the Bloch equations, we have constructed a model that describes the dynamics of the nuclear magnetisation of two noble gas isotopes. These two models are combined into one self-consistent model by taking into account the spin-exchange interaction. This theoretical model describes the basic physical processes of the physical block of the NMR-gyro. Using the obtained model, we have plotted the time dependence of the gyroscope signal. It is noted that the signal has a periodic, but complex composite structure. Determining the velocity of mechanical rotation with the required accuracy using simple demodulation methods is not possible. Thus, the analysis of the received signal shape makes it possible to formulate a future research task in this area – the development of new methods and algorithms for the demodulation of the NMR-gyro signal, which provide high accuracy. In conclusion, the gyroscope signal has been considered after passing through a synchronous detector at the EPR frequency.

Acknowledgements. This work was supported by the Ministry of Education and Science of the Russian Federation under the Federal Target Programme "Research and Development in Priority Areas of the Scientific and Technological Complex of Russia for 2014–2020" (Agreement No. 14.578.21.0211, unique identifier of the agreement, RFMEFI57816X0211).

References

1. Rabi I.I., Zacharias J.R., Millman S., Kusch P. *Phys. Rev.*, **53**, 318 (1938).
2. Pomerantsev N.M. *Usp. Fiz. Nauk*, **65**, 87 (1958).
3. Waters G.S., Francis P.D. *J. Sci. Instrum.*, **35**, 88 (1958).
4. Gabuda S.P., Pletnev R.N., Fedotov M.A. *Yadernyi magnitnyi rezonans v neorganicheskoi khimii* (Nuclear Magnetic Resonance in Inorganic Chemistry) (Moscow: Nauka, 1988).
5. Lauterbur P.C. *Nature*, **242**, 5394 (1973).
6. Maleev P.I. *Novye tipy giroskopov* (New Types of Gyroscopes) (Leningrad: Sudostroenie, 1971).
7. Simpson J.H., Fraser J.T., Greenwood I.A. *IEEE Trans. Aerosp. Support*, **1**, 1107 (1963).
8. Litmanovich Yu.A., Vershovskii A.K., Peshekhonov V.G. *Materialy plenarnogo zasedaniya 7-oi rossiiskoi mul'tikonferentsii po problemam upravleniya* (Proceedings of the Plenary Meeting of the 7th Russian Multi-conference on Management Issues) (St. Petersburg, 2014) p. 35.
9. Vershovskii A.K., Litmanovich Yu.A., Pazgalev A.S., Peshekhovov V.G. *Girosk. Navig.*, **26** (1), 55 (2018).
10. Umarhodzhaev R.M. *Radiotekh. Elektron.*, **22**, 597 (1977).
11. Greenwood I.A. United State Patent 4.403.190 (1983).
12. Kornack T.W., Ghosh R.K., Romalis M.V. *Phys. Rev. Lett.*, **95**, 230801 (2005).
13. Dong H., Fang J., Qin J., Chen Y. *Opt. Commun*, **284**, 2886 (2011).
14. Kanegsberg E.A. *Proc. SPIE*, **157**, 73 (1978).
15. Larsen M. *Mater. Conf. 'Frequency Control Symposium (FCS)'* (Baltimore, 2012) p. 1.
16. Korver A., Thrasher D., Bulatowicz M., Walker T.G. *Phys. Rev. Lett.*, **115**, 253001 (2015).
17. Meyer D., Larsen M. *Girosk. Navig.*, **1** (84), 3 (2014).
18. Walker T.G., Larsen M.S. *Adv. At. Mol. Opt. Phys.*, **65**, 377 (2016),
19. Cooper J.J., Hallwood D.W., Dunningham J.A. arXiv:1003.3587.
20. Zhang C., Yuan H., Tang Z., Quan W., Fang J.C. *Appl. Phys. Rev.*, **3**, 041305 (2016).
21. Zhang D.-W., Xu Zh.-Yi, Zhou M., Xu X.-Ye. *Chin. Phys. B*, **26**, 023201 (2017).
22. Maleev N.A., Blokhin S.A., Bobrov M.V., et al. *Girosk. Navig.*, **26** (1), 81 (2018).
23. Popov E.N., Barantsev K.A., Litvinov A.N. *Girosk. Navig.*, **24** (4), 3 (2016).
24. Popov E.N., Barantsev K.A., Ushakov N.A., et al. *Girosk. Navig.*, **26** (1), 93 (2018).
25. Opechowski W. *Rev. Mod. Phys.*, **25**, 264 (1953).
26. Cohen-Tannoudji C., Laloë F. *J. Phys.*, **28**, 722 (1967).
27. Sokolov I.M., Kuraptsev A.S., Kupriyanov D.V., et al. *J. Mod. Opt.*, **60**, 50 (2013).
28. Roof S., Kemp K., Havey M.D., et al. *Opt. Lett.*, **40**, 1137 (2015).
29. Skipetrov S.E., Sokolov I.M., Havey M.D. *Phys. Rev. A*, **94**, 013825 (2016).

30. Lindberg M., Binder R. *Phys. Rev. Lett*., **75**, 1403 (1995).
31. Happer W., Miron E., Schaefer S., et al. *Phys. Rev. A*, **29**, 3092 (1984).
32. Zeng X., Wu Z., Call T., et al. *Phys. Rev. A*, **31**, 260 (1985).
33. Popov E.N., Voskoboinikov S.P., Ustinov S.M., et al. *JETP*, **125**, 1005 (2017) [*Zh. Eksp. Teor. Fiz*., **152**, 1179 (2017)].
34. Abragam A. *The Principles of Nuclear Magnetism* (Oxford: Clarendon Press, 1961; Moscow: Inostrannaya literatura, 1963).
35. Popov E.N., Barantsev K.A., Litvinov A.N. *J. Appl. Magn. Reson*., **48**, 761 (2017).
36. Popov E.N., Barantsev K.A., Litvinov A.N. *Phys. Wave Phenom*., **24**, 203 (2016).
37. Barantsev K.A., Popov E.N., Litvinov A.N. *Quantum Electron*., **47**, 777 (2017) [*Kvantovaya Elektron*., **47**, 777 (2017)].
38. Barantsev K.A., Litvinov A.N., Popov E.N. *JETP*, **125**, 993 (2017) [*Zh. Eksp. Teor. Fiz*., **152**, 1165 (2017)].